Haptic Jamming: A Deformable Geometry, Variable Stiffness Tactile Display using Pneumatics and Particle Jamming

Andrew A. Stanley[1]* James C. Gwilliam[1,2]* Allison M. Okamura[1]
astan@stanford.edu jim.gwilliam@jhu.edu aokamura@stanford.edu

[1]Department of Mechanical Engineering, Stanford University
[2]Department of Biomedical Engineering, Johns Hopkins University

ABSTRACT

Many controllable tactile displays present the user with either variable mechanical properties or adjustable surface geometries, but controlling both simultaneously is challenging due to electromechanical complexity and the size/weight constraints of haptic applications. This paper discusses the design, manufacturing, control, and preliminary evaluation of a novel haptic display that achieves both variable stiffness and deformable geometry via air pressure and a technique called particle jamming. The surface of the device consists of a flat, deformable layer of hollow silicone cells filled with coffee grounds. It selectively solidifies in different regions when the air is vacuumed out of individual cells, jamming the coffee particles together. The silicone layer is clamped over a chamber with regulated air pressure. Different sequences of air pressure and vacuum level adjustment allow regions of the surface to display a small rigid lump, a large soft plane, and various other combinations of lump size and stiffness. Experimental data from individual cells show that surface stiffness increases with vacuum level and the elliptical shape of the cells become increasingly spherical with increased chamber pressure.

Index Terms: H.5.2 [Information Interfaces and Presentation]: User Interfaces—Haptic I/O;

1 INTRODUCTION

An ideal tactile display would be capable of controlling and transmitting multiple tactile quantities simultaneously, such as geometry, compliance, texture, and temperature. However, most tactile displays are limited in the scope of tactile sensations they can evoke, in large part because of the electromechanical complexities associated with developing devices that meet the physical constraints of many haptic applications. Researchers have developed displays optimized to display changes in surface geometry or shape (e.g., [5] [9] [11] [21]), although these displays do not allow for independent control of surface compliance. Others have developed displays that focus on controlling compliance and surface properties (e.g., [13] [22]), but do not actively control surface shape or geometry. Recently, air-jet-based tactile devices have been used to create simple displays that can control perceived geometry and surface properties simultaneously and independently [8] [10].

Distributed tactile displays that enable "encountered-type" interactions are particularly attractive because they allow users to freely explore a surface or object. Several existing tactile displays convey haptic information about virtual or remote geometries and stiffnesses without requiring the user to wear or hold onto a device. The concept of "digital clay" [18] was proposed for 3D computer input/output interfaces; several potential methods have been conceptualized for creating a controllably deformable surface, including an array of fluid-driven actuators [24]. Other approaches include tactile arrays of electrorheological [22] and magnetorheological [13] fluids, which transform material properties under application of an electric or magnetic field, respectively. The "T-PaD" (and its subsequent family of surface haptics devices) creates variable friction on a surface through ultrasonic vibrations [23]. Another surface haptics approach uses small electrostatic forces to vary surface friction [2]. Other implementations, including shape memory alloy arrays [21] and other types of pin arrays are summarized in [5].

*These authors contributed equally to this work.

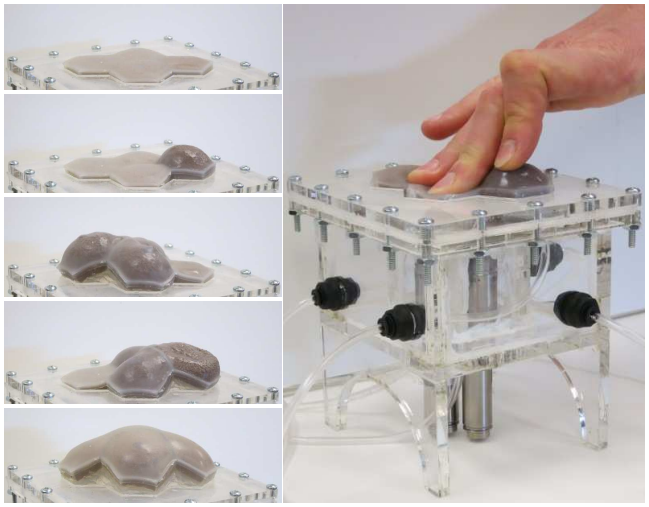

Figure 1: Haptic Jamming array prototype with four hexagonal cells.

This paper introduces a novel tactile display approach in the encountered-type and surface haptics design space. Haptic Jamming is capable of independent control of geometry and mechanical properties simultaneously using air pressure and a technique known as particle jamming. A four-cell prototype, shown in Fig. 1, uses different input sequences of air pressure beneath the cells and vacuum level adjustment within the jamming cells to allow regions of the surface to display a small rigid lump, a large soft plane, or various other combinations of lump size and stiffness.

In this paper, we review prior work in particle jamming robotics and interfaces, explain our manufacturing approach, experimentally evaluate the device's output, and provide the design of a multi-cell display. The current design is appropriate as an output device only, although it can be integrated with other components to allow user input as well. The Haptic Jamming approach has many potential applications; it was originally designed to be a component of an encountered-type combined cutaneous/kinesthetic display for medical training.

2 BACKGROUND

Particle jamming provides a method to quickly adjust the physical properties of an object. In most jamming designs, the object con-

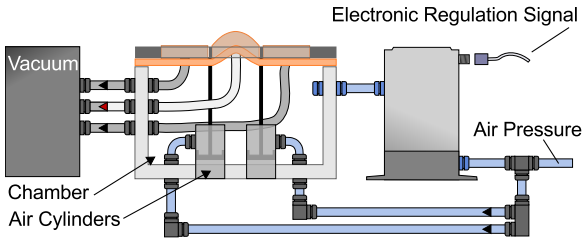

Figure 2: Setup of a Haptic Jamming device. The jamming and unjamming of individual cells to vary surface stiffness is coordinated with the pressurization of the air cylinders to pin down nodes between cells. Subsequently increasing the chamber pressure can then balloon the cells into a range of different geometries.

sists of a flexible membrane or shell filled with a granular material. When the granular material can flow freely, the object feels soft and pliable. However, when the particles are jammed together, often by vacuuming the air out of the membrane, the object feels firm and holds its current shape. Liu and Nagel [12] proposed a phase diagram for particle jamming that explains how the density, load, and temperature changes of certain materials can induce an overall increase in stiffness of the object (i.e., jamming).

Particle jamming has been explored for applications in a variety of fields. In robotics, Steltz *et al.* demonstrated that a hollow sphere made of individual jamming cells was capable of locomotion when selectively alternating the jammed state of the cells and the inflation level of the sphere [20]. Mitsuda *et al.* used particle jamming to constrain the arm of a user via a wearable force display [17]. Adjusting the vacuum state allowed the simulation of stiff or viscous virtual environments as the user moved his or her arm. Particle jamming has also been proposed for developing simpler and cheaper robotic manipulators [4] and end effectors [3]. In the medical field, jamming has been used to develop a flexible endoscope with controllable rigidity [14]. Particle jamming has also been proposed for a variety of novel user interfaces [7] [16] [1]. Other studies have focused on the physics underlying particle jamming, including experiments that test the mechanical properties of various jamming techniques and materials [6] [15], providing useful parameters for designers of future particle jamming applications. This work extends the use of the particle jamming approach into a haptic display to provide simultaneously control of both surface geometry and stiffness.

3 Methods and Materials

The Haptic Jamming display uses of a hollow layer of silicone rubber filled with a granular material (medium coarseness coffee grounds) connected to a vacuum line. Decreasing the pressure inside the silicone below ambient pressure (i.e., vacuuming) jams the granules together, stiffening the surface. The silicone layer is clamped over the top of a chamber with controllable internal air pressure. In the unjammed state, adjusting the internal pressure of the chamber causes the silicone to deform like a balloon, as illustrated in Fig. 2. Air cylinders can selectively pin down nodes between cells, as further explained in Section 5. Subsequently jamming a cell allows it to maintain its ballooned shape in a stiffened state even after the chamber pressure is released. Thus, the surface geometry of this individual cell can change independently from the mechanical properties of the surface. We first described this general approach in an abstract [19] using an alternate implementation.

Fig. 3 shows the two separate silicone pieces that form the overall structure of a Haptic Jamming device. A hollow, cylindrical silicone shell with a wall thickness of 1/16 in. fits into the flat base layer of silicone, which is 1/8 in. thick around the outside and 1/16 in. thick where the cylindrical piece fits into it. To create the molds,

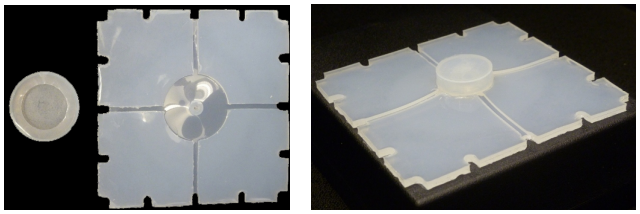

Figure 3: An empty circular silicone shell (1 inch diameter) after molding, before (left) and after (right) gluing the two parts together with Sil-Poxy.

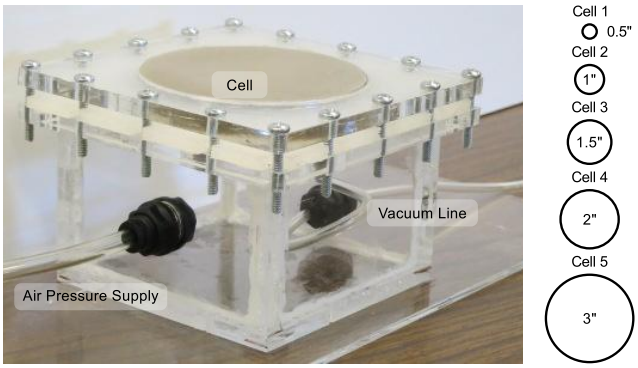

Figure 4: A single cell with chamber pressure and cell vacuum lines. Comparative cell sizes tested in this study are shown at right.

we bolted together multiple layers of laser-cut acrylic plastic, which we then filled with Ecoflex 00-30 silicone rubber (Smooth-On, Inc., Easton, PA). A 4-40 UNF threaded rod in the mold holds a space in the mold for pneumatic tubing and is easily removed after the silicone has cured. The Ecoflex silicone has a 100% Modulus of 10 psig and a 900% elongation at break, making for an extremely flexible and resilient surface. The hollow cylindrical shell of silicone includes a small lip on the bottom that allows more surface area for the two pieces to glue together using Sil-Poxy silicone adhesive (Smooth-On, Inc.).

A short extrusion around the hole in the bottom side of the base silicone layer allows us to fill the cell with coffee grounds via a funnel, and also provides increased surface area for gluing the vacuum line tubing. Cells were filled to capacity but not to the point of bulging. The overall cell thickness is 5/16 in., chosen based on experiences with earlier prototypes. (Future work will explore thinner cells.) A 1/25 in. thick polyester felt filter prevents the vacuum line from drawing the coffee grounds out of the cell. As shown in Fig. 4, the base layer of silicone lays flat across a custom acrylic chamber with a hole in the top that matches the shape and size of the cell, and a matching sheet of acrylic clamps down over the top of it, held in place by bolts around the perimeter. Through-wall nylon push-to-connect tubing connectors bring the vacuum line and the positive air pressure into the chamber. The vacuum and pressure sources maximize at 25 inHg and 125 psig (US standard units differ for vacuum and pressure), respectively, regulated by a vacuum regulator and a QB3TFEE003-S17 pressure regulator (Proportion Air, McCordsville, Indiana) with a 0.5s rise time for step pressure changes. Lines switch electronically between the pressure or vacuum sources and exhausting to atmospheric via V1A04-BW1 three-way solenoid valves (Mead Fluid Dynamics, Inc., Chicago, IL).

Prior particle jamming studies guided our selection of coffee grounds as the granular material to fill the cells. Most recently, Cheng *et al.* tested six different grains for their jamming-enabled manipulator, including coarse coffee, fine coffee, saw dust, di-

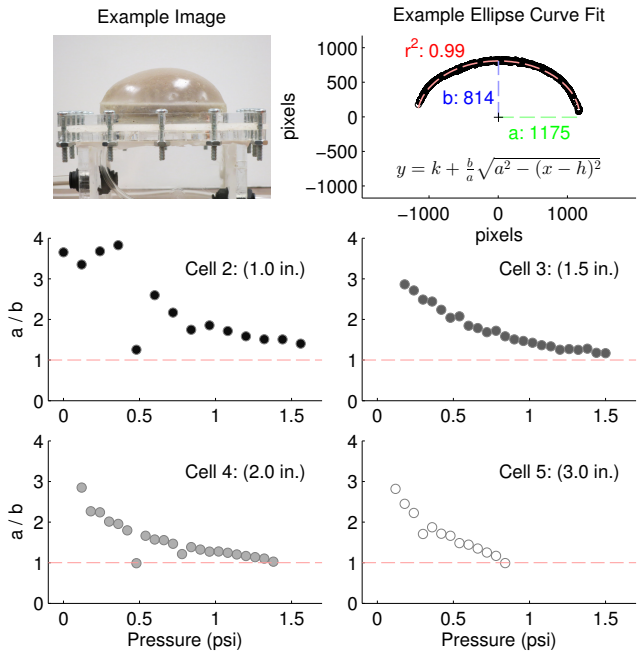

Figure 5: Effects of chamber pressure on cell geometry. (Row 1) (left) Images were taken of each cell profile at varying chamber pressures. (r) Ellipsoid curves were fit to points resulting from image edge detection. Ellipsoid fit yields major (a) and minor (b) axis measurements. (Rows 2-3) Cell eccentricity (b/a) as chamber pressure is increased. Each plot represents a different cell size.

atomaceous earth, solid glass beads, and hollow glass beads [4]. Only the modulus of the solid glass beads exceeded that of the coarse coffee, but the coffee's yield stress eclipsed that of the beads by nearly five times, possibly due to the way that the irregular shapes of the grounds helps them to lock together under vacuum.

4 Experimental Evaluation of Single Cell Units

We constructed individual circular cells of varying diameters (0.5, 1.0, 1.5, 2.0, and 3.0 in.) to test how the mechanical properties and geometric behaviors of the cells change with size, as well as to establish size limits of cells that were both functional and capable of being reliably manufactured by hand. We designed experiments to test the effects of vacuum level, chamber pressure, underlying support, and cell diameter on the performance of the display. The underlying support included three conditions, illustrated at the bottom of Fig. 8: unsupported, where the acrylic underneath the cell had a cutout that exactly matched the diameter of the cell; semi-supported, where the diameter of the cutout was slightly smaller than inner diameter of the cell wall to reach past the edge of the coffee; and supported, where the cutout was just big enough to fit the vacuum tube and silicone sleeve through it.

4.1 Geometry Characterization

The purpose of the geometry experiments was to evaluate how the shape of the particle-jamming cells changed as a function of varying chamber pressure and the vacuum state of the cell. The first experiment focused on cell shape as a function of cell size and chamber pressure, while the second experiment evaluated whether vacuuming the cell to increase its stiffness also changes its geometry.

For each cell, chamber pressure was initiated at 0 psig and increased in increments of 0.06 psig. At each pressure increment, an image of the horizontal profile of the cell shape was captured

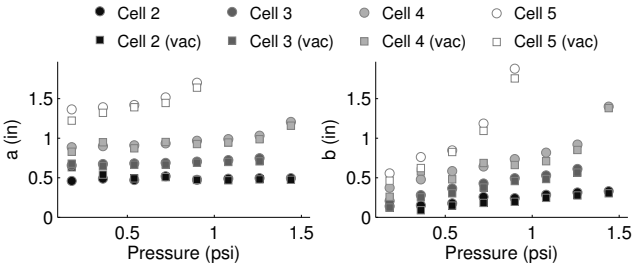

Figure 6: Effects of vacuum on cell geometry. Markers represent major (left) and minor (right) ellipsoid fit measurements across the range of chamber pressures. Markers represent the cell states after being pressurized, then either left unvacuumed (circle) or vacuumed (square). Vacuuming the cells has little effect on overall shape.

(Fig. 5, top left). Cell 1 (the smallest size) did not show any noticeable shape deformations at the maximum pressure of the regulator and was thus not included in the experimental data. For each image, Matlab's image processing toolbox was used to threshold the image by intensity and locate the boundary of the cell using the Sobel edge detection method. An ellipsoid was fit to each resulting curve using an unconstrained nonlinear minimization of the sum of squared residuals (SSR). The ellipsoid equation is given by

$$y(x) = k + \frac{b}{a}\sqrt{a^2 - (x-h)^2}, \tag{1}$$

where h and k represent the horizontal and vertical centering terms, respectively, and a and b represent the major and minor axes of the ellipsoid, respectively.

Fig. 5 (top right) shows the points constituting the cell shape boundary produced from the edge detection, as well as the resulting ellipsoid fit, with coefficient of determination (r^2), and major (a) and minor (b) ellipsoid axes. The same analysis was repeated at each pressure increment for every cell size, yielding r^2 greater than 0.95 in 75% of the measurements. The remaining plots in Fig. 5 show how the shape of each cell changes as a function of increasing chamber pressure. Two observations can be made from these data: First, cell shape is elliptical at low pressures and becomes increasingly circular as the chamber pressure is increased. Second, larger cells reach a full circular shape at lower pressures than smaller cells.

Fig. 6 illustrates how vacuuming each cell affects its shape. Both major (a) and minor (b) axis lengths are shown as cell size and chamber pressure are varied. Circular and square markers indicate the fit ellipse axis values when the chamber is pressurized and subsequently after the cell is vacuumed, respectively. Vacuuming the cell has little effect on the overall shape of the cell. The most noticeable effect occurs in the minor axis measurement (b), particularly in the larger cells, which flatten mildly as they are vacuumed. Subsequent release of chamber pressure does not affect the cell geometry, but does lower the position of the horizontal axis flush with the acrylic surface. As demonstrated in the accompanying video, any external deformation of the cell will be fixed during vacuuming, allowing the user to mold custom shapes. However, this feature also prohibits controllable change in configuration during user contact.

4.2 Mechanical Properties Characterization

To test the mechanical properties of these cells in various configurations, we attached an ATI Nano17 force/torque sensor (ATI, Apex, NC) to the end effector of a Sensable Phantom Premium (SensAble Technologies, Inc., Wilmington, MA) and manually pushed on the display. The Phantom provided force feedback to keep the end effector centered above the middle of the cells and also collected position data along the vertical axis of movement. While we

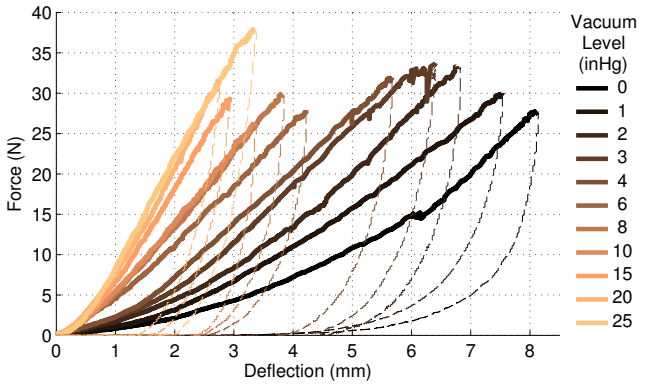

Figure 7: Force-displacement curves of a cell supported from underneath by acrylic at various levels of vacuum. Releases are shown dash-dotted.

do not anticipate users pressing on Haptic Jamming devices in our envisioned application with much more force than the force output limit of a Phantom (about 6N), we manually pushed with much higher forces in these experiments to provide further insight into the force-deflection curves of the display.

The first experiment aimed to determine the effect of vacuum level on cell stiffness. We set up the largest cell in the fully supported configuration and pushed halfway between the center and the edge of the cell to avoid any boundary effects from the cell wall or tubing. The force-displacement curves from this experiment at several vacuum levels are shown in Fig. 7. As expected, increasing the level of vacuum leads to an increase in (nonlinear) cell stiffness as the coffee grounds inside jam together with greater force. All curves show strong hysteresis, with force plummeting almost all the way back to zero upon initial release. We attribute this hysteresis to the tendency of coffee grounds to hold shape unless disturbed by an external force; in this case no external force acts on the grounds during the release other than comparatively weak force of the silicone rebounding from a compressed state. At vacuum levels greater than 1 inHg, the jammed coffee stiffened sufficiently to keep the cell surface fully deformed despite the rebounding of the silicone. We leave the development and validation of a complete mechanical model to future work.

The next experiment sought to clarify the role that the type of support underneath the cell plays in the forces displayed to the user. As it proved difficult to isolate this variable, we tested all three of the support types in nine different arrangements, as shown in Fig. 8. The release phases of each curve, which dropped to zero in a similar fashion to those in Fig. 7, are omitted for clarity. For each support type and for three different chamber pressures (0, 0.6, 1.2 psig), we applied force to the 1.5 in. diameter cell in each of three configurations. These involved pressing after pressurizing the chamber but before vacuuming the cell, after vacuuming the cell with the chamber still pressurized, and after depressurizing the chamber with the cell vacuumed solid in its inflated shape. As one might expect, increasing the amount of support underneath the cell increased the force required to displace the cell. However, these effects decreased as the chamber pressure increased because the pressurization pushed the cell upward off of the support surface. At high enough chamber pressures, the support type plays almost no role in the force a user would feel, except when an un-vacuumed cell is deflected deep enough to "bottom out" on the full support, at which point the stiffness of the acrylic dominates. At low chamber pressures, the force of the silicone stretching dominates unless the cell is supported.

We conducted a third experiment to examine the effects of chamber pressure and cell size on the mechanical properties of single cells. For each of the four cell diameters and at each of several levels of chamber pressure, we collected force-displacement curves before and after completely vacuuming the cell. Fig. 9 contains the results of these tests. When cells were fully vacuumed, neither cell size nor chamber pressure played a significant role in the stiffness of the cell as the forces from all trials closely matched for the first

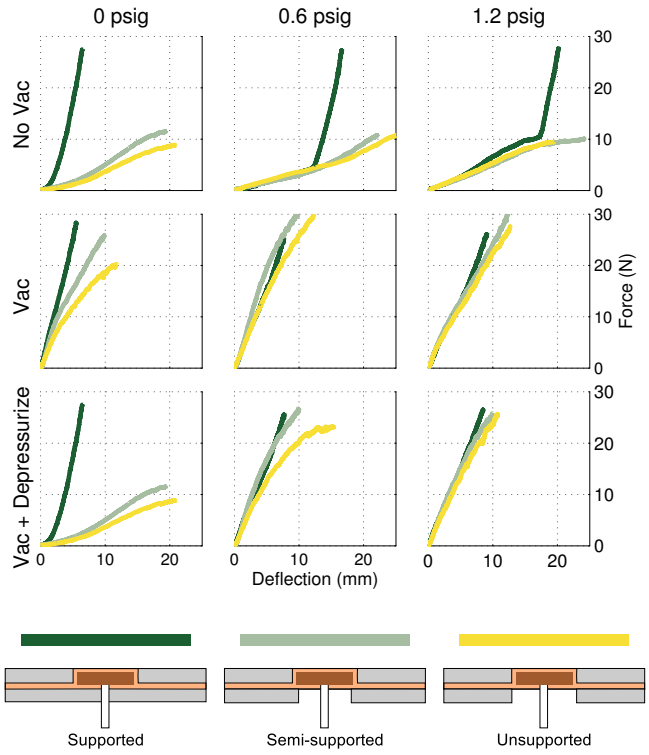

Figure 8: Force deflection curves obtained from 1.5" diameter cell under three different states with varying support conditions. States include an un-jammed pressurized cell (No Vac), a jammed pressurized cell (Vac), and a jammed depressurized cell (Vac + Depressurize). The support condition affects mechanical properties less as pressure in the cell is increased.

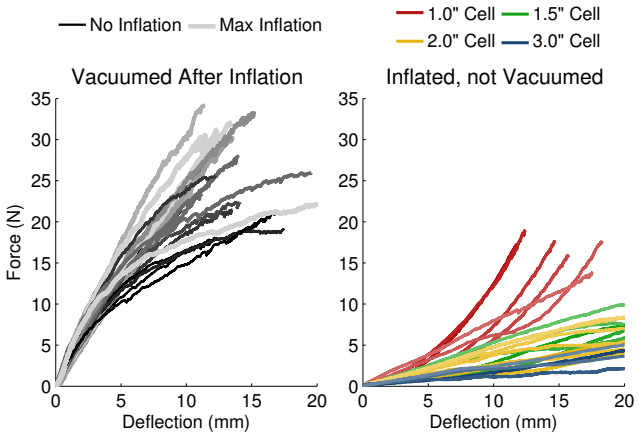

Figure 9: Left: Force-deflection curves of cells of all sizes at various pressures after vacuuming. Lighter shades indicate higher chamber pressures. Right: Force deflection curves before vacuuming the cells, color coordinated by cell size.

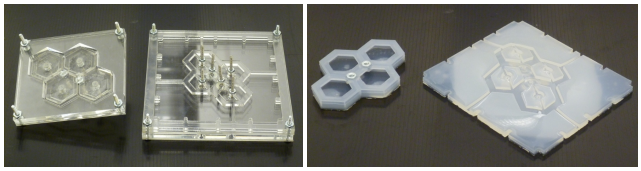

Figure 10: Left: The acrylic molds used to manufacture the array. Right: Empty silicone cells after molding.

few millimeters of deflection. At higher forces, however, the coffee yielded and deformed around the ball on the tip of the Phantom end effector. For most trials, increasing the pressure and ballooning the cell more before vacuuming led to a higher yield force as the arched shape strengthened the overall structure of the lump. When cells were not vacuumed, the stiffness of the soft lump depended more on the cell diameter than the chamber pressure. Smaller cells required greater deflection of the outer silicone cell edges per each millimeter of depth, resulting in higher forces.

5 A Multi-Cell Array to Display More Complex Geometries

An array of multiple Haptic Jamming cells opens the door to display a variety of geometries beyond simple ellipsoids. Toward this end, we constructed a four-cell prototype to demonstrate the feasibility of combining multiple cells to display lumps of varying sizes and stiffnesses from a single surface array.

5.1 System Setup

The Haptic Jamming approach was initially constructed as a variable lump display for medical simulation applications. Accordingly, we selected hexagonal cells since they are the closest to circular amongst the family of shapes that tessellate without gaps. Similar to the individual circular cells, we molded the silicone rubber sheet out of two separate pieces poured into custom-designed layered acrylic cutouts. Each hexagon in this prototype measures 0.675 in. per side. In addition to the four hexagonal cells, two 5-40 nuts are embedded in the silicone at each of the two internal nodes between the cells. The rods of two Airpot Airpel E9 air cylinders (Airpot, Norwalk, CT) are aligned directly below the two nodes and screw into these nuts. When the air cylinders are not pressurized, the rods move up and down freely with the motion of the silicone layer as it deforms. Pressurizing the top of an air cylinder forces the piston and rod downward, effectively pinning the node to stay level with the flat surface of the surrounding acrylic. Two washers attach to the bottom surface of the silicone with Sil-Poxy to prevent the forces of the air cylinders from pulling the embedded nuts through the holes for the rods in the silicone base layer.

Six of the same three-way solenoid valves are used to control each of the four vacuum lines to the cells as well as the two pressurized lines to the air cylinders individually. A USBDUX DAQ (Linux-USB-DAQ, Sterling, United Kingdom) toggles the signal voltages to the bases of six 2N3904 NPN bipolar junction transistors (Fairchild Semiconductor, San Jose, CA) to open and close the solenoid valves electronically. A customized graphical user interface to the DAQ also sets the analog voltage signal to the pressure regulator to control the pressure inside the main chamber. Fig. 11 shows a block diagram describing the full system setup.

5.2 Increased Variability of Geometry

The use of the air cylinders allows the display of a number of different geometries even before exercising the capabilities of the particle jamming technology. Pressurizing both air cylinders while the surface is inflated, for example, changes the surface from one large lump to four separate smaller lumps. Subsequently releasing one of

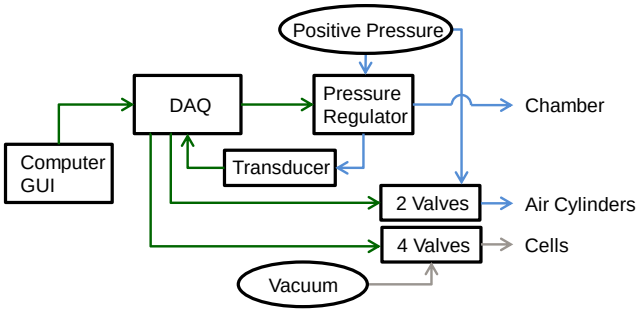

Figure 11: A block diagram of the system setup. Electronic connections are shown in dark green, positive air pressure in light blue, and vacuum in gray.

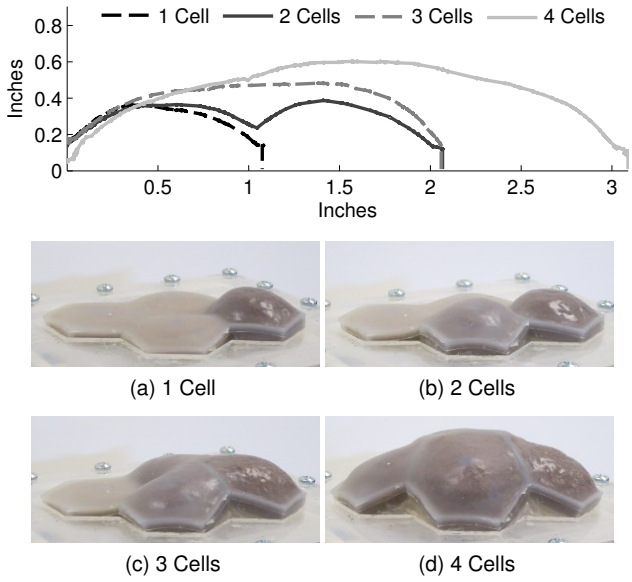

Figure 12: Top: A sample of geometry profile shapes obtainable with Haptic Jamming. Bottom: In all images (a-d), the chamber was pressurized, the raised cells were vacuumed, then the chamber was depressurized. Vacuuming a cell results in a darker shade.

the air cylinders leaves one of these small lumps alongside a larger lump from the combination of the three other cells. Vacuuming the cells in any configuration converts the surface from soft to stiff.

Altering the order in which cells, air cylinders, and the main chamber are jammed, unjammed, pressurized, and exhausted reveals an assortment of other forms the surface can assume. For example, the sequence of jamming three of the four cells, pressurizing both air cylinders to pin down the nodes, increasing the main chamber pressure to balloon the unjammed cell, jamming the ballooned cell, reducing the main chamber pressure, unjamming the other three cells, and releasing the air cylinders results in a single stiff lump the size of one cell surrounded by soft cells, as shown in Fig. 12a. Figs. 12b - 12d illustrate that similar processes can create individual lumps from two, three, or all four cells, respectively, by adjusting which cells are vacuumed and which air cylinders are pressurized. The graphical user interface includes buttons to run through each of these sequences automatically, with intervals timed to provide adequate chamber inflation and cell vacuuming. The video that accompanies this paper demonstrates the system in action, creating lumps of various shapes, stiffnesses, and sizes in the order of seconds or milliseconds.

As the experiment in Section 4 shows, the size and stiffness of any of these lumps can be controlled with the internal chamber pressure and vacuum levels. Fig. 12 illustrates a subset of the geometries the display is capable of producing, captured using the same image analysis techniques described in Section 4.

6 Conclusions and Future Work

This paper presented a novel tactile display capable of generating a variety of surface geometries over a range of stiffnesses under automatic control using the technique of particle jamming. Particle jamming has proven an effective tool in a variety of robotics applications and now shows promise to add another dimension to the versatility of haptic displays. A set of experiments testing surface shapes and force-deflection curves provides extensive insight into the range of user interactions such a display could effectively provide, given the design and manufacturing techniques described in this paper. This type of variability in a tactile display could prove useful for applications ranging from medical simulation to tactile feedback in teleoperation. This paper also discussed a preliminary prototype of a particle jamming surface array with four cells that implemented a pair of air cylinders to pin down the nodes between cells to allow an even greater variety of surface geometry.

Increasing the number of cells in and overall size of a particle jamming surface array promises to provide even greater geometric variability and resolution. We are currently working toward creating a larger array capable of providing this improved variability and resolution. To create smaller cells and larger arrays may require testing thinner cells and developing an alternate method for pinning down the nodes between cells, possibly with miniature solenoids or motors. We also aim to develop a full, data-driven dynamic model of particle jamming cells to accurately predict the forces and geometries a surface will display under any given configuration. This dynamic model should allow more precise control of the automated system.

An additional avenue worth considering involves connecting another vacuum line to the main chamber. This would allow cells to cave downward with negative gauge pressure. Surrounding a cell that protrudes upward with a ring of cells depressed downward could make for a more compelling lump display. Redesigning the boundaries of the cell could mitigate the rising and falling of the surface resulting from chamber pressure changes. Adding a membrane over the surface of the display could be appropriate for displaying lumps embedded within tissue. Ultimately we plan to integrate this tactile display with a larger encountered-type haptic interface that utilizes a robotic cable-driven platform to expand the workspace and apply kinesthetic forces. Combining these devices will allow the rendering of complex virtual environments with both cutaneous and kinesthetic haptic feedback that the user can interact with directly using his or her own hands.

Acknowledgements

This work was supported by U.S. Army Medical Research and Materiel Command (USAMRMC; W81XWH-11-C-0050) to AMO and by the National Science Foundation Graduate Research Fellowship Program to AAS and JCG. The authors thank T. N. Judkins and J. E. Colgate for their help in concept development.

References

[1] N. Aihara, T. Sato, and H. Koike. Highly deformable interactive 3D surface display. In *Proc. ACM Symposium on User Interface Software and Technology*, pages 91–92, New York, New York, USA, 2012.

[2] O. Bau, I. Poupyrev, A. Israr, and C. Harrison. TeslaTouch: electrovibration for touch surfaces. In *Proc. ACM Symposium on User Interface Software and Technology*, pages 283–292, 2010.

[3] E. Brown, N. Rodenberg, J. Amend, A. Mozeika, E. Steltz, M. R. Zakin, H. Lipson, and H. M. Jaeger. Universal robotic gripper based on the jamming of granular material. *Proceedings of the National Academy of Sciences*, 107(44):18809–18814, 2010.

[4] N. G. Cheng, M. B. Lobovsky, S. J. Keating, A. M. Setapen, K. I. Gero, A. E. Hosoi, and K. D. Iagnemma. Design and analysis of a robust, low-cost, highly articulated manipulator enabled by jamming of granular media. In *Proc. IEEE International Conference on Robotics and Automation*, pages 4328–4333, 2012.

[5] V. G. Chouvardas, A. N. Miliou, and M. K. Hatalis. Tactile displays: Overview and recent advances. *Displays*, 29(3):185–194, 2008.

[6] E. I. Corwin, H. M. Jaeger, and S. R. Nagel. Structural signature of jamming in granular media. *Nature*, 435(7045):1075–8, 2005.

[7] S. Follmer, D. Leithinger, A. Olwal, N. Cheng, and H. Ishii. Jamming user interfaces: programmable particle stiffness and sensing for malleable and shape-changing devices. In *Proc. ACM Symposium on User Interface Software and Technology*, pages 519–528, 2012.

[8] J. C. Gwilliam, A. Degirmenci, M. Bianchi, and A. M. Okamura. Design and control of an air-jet lump display. In *Proc. IEEE Haptics Symposium*, pages 45–49, 2012.

[9] R. Howe, W. Peine, D. Kantarinis, and J. Son. Remote Palpation Technology. *IEEE Engineering in Medicine and Biology Magazine*, 14(3):318–323, 1995.

[10] K. Inoue, F. Kato, and S. Lee. Haptic device using flexible sheet and air jet for presenting virtual lumps under skin. In *Proc. IEEE International Conference on Intelligent Robots and Systems*, pages 1749–1754, 2009.

[11] C.-H. King, M. O. Culjat, M. L. Franco, J. W. Bisley, E. Dutson, and W. S. Grundfest. Optimization of a pneumatic balloon tactile display for robot-assisted surgery based on human perception. *IEEE Transactions on Biomedical Engineering*, 55(11):2593–2600, 2008.

[12] A. J. Liu and S. R. Nagal. Jamming is not just cool any more. *Nature*, 396:21–22, 1998.

[13] Y. Liu, R. Davidson, P. Taylor, J. Ngu, and J. Zarraga. Single cell magnetorheological fluid based tactile display. *Displays*, 26(1):29–35, 2005.

[14] A. J. Loeve, O. S. Ven, J. G. Vogel, P. Breedveld, and J. Dankelman. Vacuum packed particles as flexible endoscope guides with controllable rigidity. *Granular Matter*, 12(6):543–554, 2010.

[15] T. Majmudar, M. Sperl, S. Luding, and R. Behringer. Jamming transition in granular systems. *Physical Review Letters*, 98(5), 2007.

[16] A. Mazzone, C. Spagno, and A. Kunz. The HoverMesh: A deformable structure based on vacuum cells. In *Proc. ACM SIGCHI International Conference on Advances in Computer Entertainment Technology*, pages 187–193, 2004.

[17] T. Mitsuda, S. Kuge, M. Wakabayashi, and S. Kawamura. Wearable force display using a particle mechanical constraint. *Presence: Teleoperators and Virtual Environments*, 11(6):569–577, 2002.

[18] J. Rossignac, M. Allen, W. Book, A. Glezer, I. Ebert-Uphoff, C. Shaw, D. Rosen, S. Askins, P. Bosscher, J. Gargus, I. Llamas, and A. Nguyen. Finger sculpting with Digital Clay: 3D shape input and output through a computer-controlled real surface. In *Proc. Shape Modeling International*, pages 229–231, 2003.

[19] A. A. Stanley, J. C. Gwilliam, T. N. Judkins, and A. M. Okamura. A haptic display for medical simulation using particle jamming. In *Proc. Medicine Meets Virtual Reality 20*, 2013.

[20] E. Steltz, A. Mozeika, N. Rodenberg, E. Brown, and H. Jaeger. JSEL: Jamming Skin Enabled Locomotion. In *Proc. IEEE International Conference on Intelligent Robots and Systems*, pages 5672–5677, 2009.

[21] P. Taylor, A. Moser, and A. Creed. A sixty-four element tactile display using shape memory alloy wires. *Displays*, 18(3):163–168, 1998.

[22] P. Taylor, D. Pollet, A. Hosseini-Sianaki, and C. Varley. Advances in an electrorheological fluid based tactile array. *Displays*, 18(3):135–141, 1998.

[23] L. Winfield, J. Glassmire, J. E. Colgate, and M. Peshkin. T-PaD: Tactile Pattern Display through Variable Friction Reduction. In *Proc. Haptic Interfaces for Virtual Environment and Teleoperator Systems*, pages 421–426, 2007.

[24] H. Zhu and W. J. Book. Control Concepts For Digital Clay. In *Proc. 7th IFAC Symposium on Robot Control*, volume 2, pages 347–352, 2003.